

Synthesis and Characterization of Vanadium Doped Hexagonal Rubidium Tungsten Bronze

Hasina Akhter Simol^{1,4}, Istiak Hossain¹, Tapas Debnath^{2*}, Pradip K. Bakshi¹, Rumana Akther Jahan⁴, Claus H. Rüscher³ and Altaf Hussain^{1,5}

¹Department of Chemistry, University of Dhaka, Dhaka-1000, Bangladesh

²Department of Theoretical and Computational Chemistry, University of Dhaka

³Institute of Mineralogy, Leibniz University of Hannover, Callinstrasse 3, 30167 Hannover

⁴Centre for Advance Research in Sciences, University of Dhaka, Bangladesh

⁵Bangabandhu Sheikh Mujibur Rahman Maritime University, Dhaka, Bangladesh

(Received : 4 October 2023; Accepted : 13 December 2023)

Abstract

Attempts have been made to synthesize vanadium doped rubidium hexagonal tungsten bronzes with the nominal composition $Rb_xV_yW_{1-y}O_3$ ($x = 0.30, 0.25$, and $0.0 \leq y \leq x$). The samples were synthesized using the solid state synthesis method in a silica glass tube under vacuum at (10^{-2} Torr) 700°C . The X-ray diffraction measurements reveal that a pure hexagonal tungsten bronze (HTB) phase can be formed with a 60% replacement of W^{5+} by V^{5+} . The systematic incorporation of vanadium into the HTB lattice, as well as the reduction of V/W-O bond lengths in the xy plane and the lengthening of these bonds in the crystallographic c direction, are also revealed by Rietveld structure refinement of XRD data. The XRD results are supported by FTIR absorption spectra of the oxidized phases. Furthermore, an absorption signature develops as a function of y and exhibits a considerable increase in intensity with the eventual replacement of W^{5+} by V^{5+} , showing a large decrease in the metallic like contribution and revealing the compounds' nonmetallic nature. Elemental analysis indicates good agreement with nominal values, demonstrating that vanadium was systematically incorporated into the $Rb_xV_yW_{1-y}O_3$ system.

Keywords: Hexagonal tungsten bronze, Tungsten oxide, Vanadium oxide, Rubidium oxide.

I. Introduction

Tungsten bronzes, A_xWO_3 , are a series of non-stoichiometric ternary metal oxides where A is an electropositive metal atom or hydrogen and x can vary in the range $0 < x < 1$. Because of their fascinating structural, electronic, superconducting, optical, and electrochromic properties, they have been the subject of much investigation for a very long time¹⁻⁵. Due to the high NIR optical absorption capability and strong X-ray attenuation ability of alkali metal tungsten bronzes, A_xWO_3 , the possibility of their application as dual-modal contrast agent for photoacoustic tomography and X-ray computed tomography imaging as well as in the cancer therapy was discussed, recently^{6,7}.

There are four main structure types that tungsten bronzes can take based on the size of the interstitial atom, their amount (x), and preparation method. They are Perovskite Tungsten Bronzes (PTB)^{8,9}, Tetragonal Tungsten Bronzes (TTB)¹⁰, Hexagonal Tungsten Bronzes (HTB)¹¹ and Intergrowth Tungsten Bronzes (ITB)¹². These bronzes have a three-dimensional WO_3 lattice structure that is built up of WO_6 octahedra that share corners to create different types of tunnels that which are where the metal atoms are found. Among the alkali metals HTB phases are formed only by K, Cs, and Rb. In HTB, along the c-direction, the structure has hexagonal and trigonal tunnels and the interstitial atoms mainly occupy the hexagonal tunnels. The tungsten atoms

lie on the same plane; however, they are slightly displaced from the center of octahedra normal to the hexagonal axis. Because the displacement in adjacent layers is in the opposite direction, the c axis is doubled and the unit cell comprise two layers. The homogeneity range of alkali metal in HTB A_xWO_3 were reported for $0.19 < x < 0.33$ ^{13,14}.

When all of the alkali atom positions in the hexagonal tunnels are occupied, $x = 0.33$ occurs. The lower stability limit, however, has been observed to be highly dependent on preparation conditions and can be increased up to $x = 0.15$ ¹⁵. According to Hussain et al.¹⁶, the empirical formula tungsten bronzes, A_xWO_3 , may be expressed as $A_xW^{5+}_xW^{6+}_{1-x}O_3$, which shows the degree of reduction of the bronzes depends on the value of x. W^{5+} can be partly or entirely substituted by other pentavalent metal ions, or even by lower valent atoms¹⁶⁻²³ with acceptable sizes to prepare isostructural phases of partly or completely oxidized bronzes. The completely oxidized isostructural phases are termed as bronzoids²⁴.

The optical, electrical as well as magnetic properties of tungsten bronzes systematically change with systematic substitution of W^{5+} by other ions. Based on the content, x, of interstitial metal atoms, A, bronzes show metallic like electrical conductivity and superconducting properties²⁵⁻²⁹, whereas bronzoids show electrical insulating and ferroelectric properties^{30,31}. Literature survey shows that many properties like anisotropy in optical properties,

* Author for correspondence. e-mail: debnath@du.ac.bd

superconductivity and semiconductor-metallic like electrical transition of tungsten bronzes are still arguable. To explain these properties the free carrier concept^{16,32,33} and polaron concept³⁴⁻³⁶ are discussed in the literature. Besides, attempts were taken to tailor or control the properties by controlling reduction conditions through replacement of W^{5+} of tungsten bronzes by other pentavalent ions. In our earlier works, we have reported the replacement of W^{5+} in Na-PTB cubic and K-TTB, Cs-HTB phases by Nb^{5+} , and in K-HTB phase by V^{5+} and Ta^{5+} ^{19,23}. There is, however, no report on the replacement of W^{5+} in hexagonal Rb_xWO_3 by V^{5+} so far. Therefore, in the present study efforts were made to prepare vanadium doped hexagonal rubidium tungsten bronze, $Rb_xV_yW_{1-y}O_3$, having nominal compositions, $x = 0.30, 0.25$ and $0.0 \leq y \leq x$ for the first time. Moreover, vanadium based oxides exhibit diverse physicochemical properties due to its formation of wide range of V-O coordination polyhedral. Many applications such as usages as cathode materials for lithium ion batteries, thermochromic material for smart energy-saving windows, photoelectric materials, gas sensor materials, catalysts for the oxidation of organics, etc are discussed in the literature³⁷.

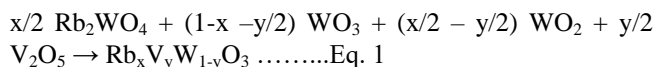
Similarly, tungsten based oxides materials also show many physiochemical properties analogous to vanadium based oxides. Therefore, synthesis and characterization of $Rb_xV_yW_{1-y}O_3$ will have the possibility to understand how vanadium doping affects superconducting, electrical conductivity, electrochromic properties, etc. which could lead to the development of more effective functional materials.

II. Experimental

Starting materials were reagent grade rubidium carbonate, tungsten (VI) oxide, (99.998 % pure; Alfa Aesar), tungsten (IV) oxide (99.9 % pure; Alfa Aesar), vanadium (V) oxide (99.998 % pure; Alfa Aesar). Reagent grade rubidium carbonate and tungsten (VI) oxide were heated at 100°C and 700°C, respectively for overnight before use. Rubidium tungstate, Rb_2WO_4 , was prepared by heating equimolar mixture of Rb_2CO_3 and WO_3 in an open crucible at 750°C for 24 hours. Using XRD and FTIR, the purity of the Rb_2WO_4 was examined.

Two series of polycrystalline samples of vanadium substituted hexagonal rubidium tungsten bronze with nominal compositions $Rb_{0.30}V_yW_{1-y}O_3$ ($0.00 \leq y \leq 0.30$) and $Rb_{0.25}V_yW_{1-y}O_3$ ($0.00 \leq y \leq 0.25$) were prepared using traditional solid state method in evacuated SiO_2 glass ampoules. Appropriate amount of the reactants was taken according to the Eq.1 and thoroughly mixed in an agate mortar and placed into dried silica glass tubes with an inner diameter of 6.0 mm and a length of around 100 mm long, preheated at 700°C for overnight). The samples tubes were then evacuated at 10^{-2} Torr at room temperature by means of

mechanical pump for two hours before sealing. The prepared reaction tubes were heated isothermally in a Muffle furnace at 700°C for 4 days and finally quenched in water within few seconds after the tubes taken out from the Muffle furnace.



The samples X-ray powder diffraction data were acquired using a Bragg-Brentano geometry on a Bruker D8 diffractometer (CuK α radiation) containing a secondary Ni filter and an X'Celerator multi-strip detector. The experiment was performed at room temperature in the 10° to 120° 2 θ range using step size of 0.02° and a data collection duration 25s/step. The structures were refined with the Rietveld program 'Diffrac Plus Topas-4.2' (Bruker AXS, Karlsruhe, Germany). Basic parameters based on experimental data determined from conventional LaB6 measurements were utilized to generate the reflex profile. A polarization parameter was fixed and the sample displacement of the center was varied as an extra general parameter. Starting atomic coordinates were taken from results Gesing et al.³⁸. The occupancy of V in the 6g site was constrained so that occ. [V] = 1- occ.[W].

In a vacuum, with a Bruker 80v FT-IR spectrometer, infrared absorption spectra were acquired. 1.0 mg of the finely powdered material was mixed with 199 mg of potassium bromide (KBr) to make a pellet with a diameter of 13 mm in order to conduct IR spectroscopic measurements (in the range of 370-5000 cm⁻¹). The spectrum of a similarly manufactured, pure KBr pellet was employed as a reference. SEM-EDX was used in this work for studying the morphology and the elemental composition of the samples of the series $Rb_{0.30}V_yW_{1-y}O_3$. Measurements were conducted using a JEOL JSM 6490 LA instrument equipped with an EDX detector operated at an accelerating voltage 20 kV. The powdered samples were smeared on adhesive carbon films and coated with platinum by vacuum sputtering method. The EDX spectra were collected in the range of 0-20 keV. The microanalyses revealed Rb:W and Rb:V:W ratios in at.%. In the quantification the entire spectra were employed. About 10 to 12 measurements were carried out in each sample and the mean values of Rb/W (= x) and V/(V+W) (=y) are considered. To check the homogeneity of the elemental compositions a line EDX scan was performed in single crystal.

III. Results and Discussion

Study of the X-ray diffraction data of powder samples

The XRD patterns of the polycrystalline samples with nominal compositions $Rb_{0.30}V_yW_{1-y}O_3$ ($0.0 \leq y \leq 0.30$) and $Rb_{0.25}V_yW_{1-y}O_3$ ($0.0 \leq y \leq 0.25$) are depicted in Figs. 1 and

2, respectively. All the X-ray diffraction peaks of samples with $x = 0.30$, $0.0 \leq y \leq 0.18$ and $x = 0.25$, $0.0 \leq y \leq 0.15$ could be indexed as HTB type phase.

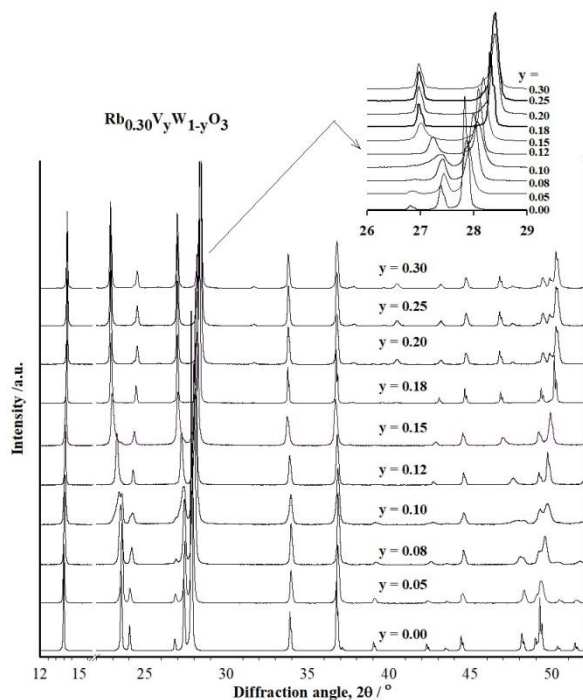


Fig. 1. XRD pattern of $\text{Rb}_{0.30}\text{V}_y\text{W}_{1-y}\text{O}_3$ ($0.0 \leq y \leq 0.30$) prepared at 700°C .

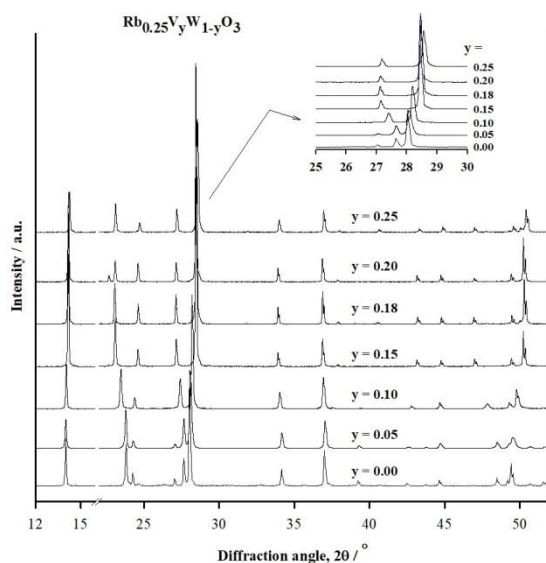


Fig. 2. The XRD pattern of $\text{Rb}_{0.25}\text{V}_y\text{W}_{1-y}\text{O}_3$ ($0.0 \leq y \leq 0.25$) prepared at 700°C .

It is observed that the diffraction lines are systematically shifted with increasing nominal vanadium content. This shift is significant up to nominal composition $y = 0.18$ for $\text{Rb}_{0.30}\text{V}_y\text{W}_{1-y}\text{O}_3$ series and $y = 0.15$ for $\text{Rb}_{0.25}\text{V}_y\text{W}_{1-y}\text{O}_3$ series. These shifts are associated with the change in the

values of the cell parameters which is a function of vanadium content, y . The XRD pattern of samples with nominal compositions $x = 0.30$, $0.20 \leq y \leq 0.30$ and $x = 0.25$, $0.18 \leq y \leq 0.25$ show presence of some weak reflection other than bronze type, which, however, unable to be indexed as HTB. The cell parameters were refined (selecting the peaks related HTB phase only) using space group $\text{P6}_3/\text{mcm}$ (No. 193). Rietveld refinement fit of some of the selected samples of the $\text{Rb}_{0.30}\text{V}_y\text{W}_{1-y}\text{O}_3$ ($0 \leq y \leq 0.30$) solid-solution series are shown in Fig. 3. Table 1 shows the cell parameters acquired via Rietveld refinement of all samples and cell parameter variations as a function of vanadium content, y , for $\text{Rb}_{0.30}\text{V}_y\text{W}_{1-y}\text{O}_3$ and $\text{Rb}_{0.25}\text{V}_y\text{W}_{1-y}\text{O}_3$ are plotted in Fig.4a and Fig.4b respectively.

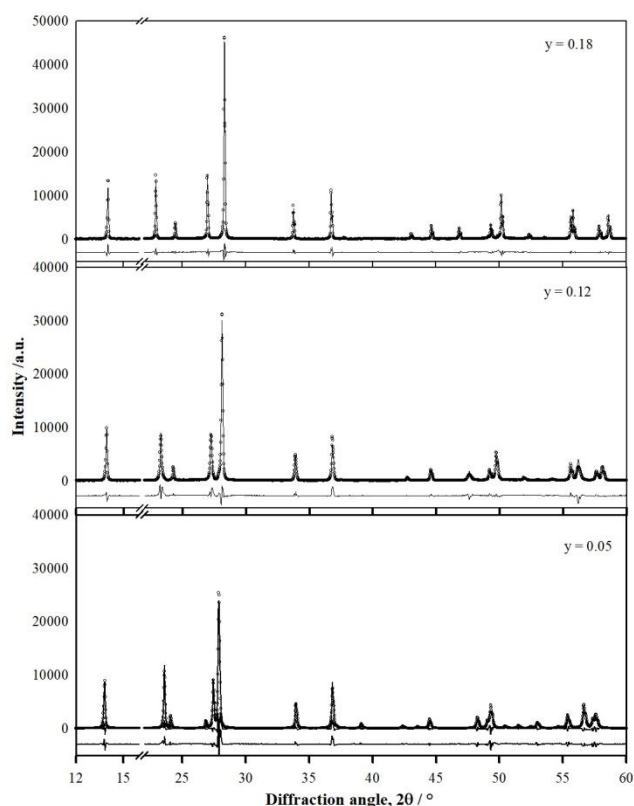


Fig. 3. Rietveld refinements fit three selected samples of the $\text{Rb}_{0.30}\text{V}_y\text{W}_{1-y}\text{O}_3$ ($0.0 \leq y \leq 0.30$) series. The observed/measured spectrum are represented by dots, and the calculated data represented by line across the dots. The curve below the spectrum represents the difference spectrum.

It has been observed that the lattice parameter a decrease up to $y = 0.18$, and then remains constant as y increases further, but c slightly decreases up to $y = 0.05$, then increases linearly as y increases from 0.05 to 0.18 for the series $\text{Rb}_{0.30}\text{V}_y\text{W}_{1-y}\text{O}_3$ ($0 \leq y \leq 0.30$). However, cell parameters a and c remain nearly constant with further

increase in y . The cell volume shows an overall decreasing trend with increasing vanadium content. These results also support our previous report on vanadium doped hexagonal potassium tungsten bronze²³.

Table 1. List of cell parameters obtained after Rietveld refinement of X-ray diffraction data.

	Nominal content, y	Cell parameters (Å)	
		a	c
$\text{Rb}_{0.30}\text{V}_y\text{W}_{1-y}\text{O}_3$	0.00	7.39217 (5)	7.55256(7)
	0.05	7.38131(12)	7.53589(14)
	0.08	7.35425(17)	7.56402(21)
	0.10	7.33812(41)	7.59420(51)
	0.12	7.32642(13)	7.63470(17)
	0.15	7.30424(21)	7.72290(28)
	0.18	7.268166(73)	7.75000(11)
	0.20	-----	-----
	0.25	7.25171(20)	7.75735(30)
	0.30	7.25237(22)	7.75704(30)
$\text{Rb}_{0.25}\text{V}_y\text{W}_{1-y}\text{O}_3$	0.00	7.39866 (8)	7.53460(9)
	0.05	7.38165 (9)	7.52670(11)
	0.10	7.33719(10)	7.62235(12)
	0.15	7.27097(9)	7.75753(11)
	0.18	7.27099(12)	7.75753(15)
	0.20	7.28161(21)	7.75872(32)
	0.25	7.26202(18)	7.75903(25)

Similar results are also obtained for the series $\text{Rb}_{0.25}\text{V}_y\text{W}_{1-y}\text{O}_3$ ($0 \leq y \leq 0.25$) shown in Fig.4b. In this series, however, the cell parameters remain nearly constant for the compositions $0.15 < y \leq 0.25$. Thus, the significant change in lattice parameters indicates the formation of solid solution series $\text{Rb}_x\text{V}_y\text{W}_{1-y}\text{O}_3$ having HTB type structure through the substitution of tungsten by vanadium in Rb_xWO_3 . Moreover, the observed overall decrease of the cell parameter a and increase in of the cell parameter c when W^{5+} are partially replaced by V^{5+} indicates that the distances between tungsten atoms within the xy hexagonal plane become smaller (WO_6 octahedra are more ‘squeezed’) and the distances between the tungsten atoms in the c direction increase. It is also observed that extent of squeezing of WO_6 octahedra depends on the vanadium content. But certainly, there is a limiting value of squeezing which reaches lowest for $y = 0.18$ composition. Similarly, the distances between the tungsten atoms along the crystallographic c direction increases with increasing nominal vanadium content and reaches to maximum value for $y = 0.18$ composition.

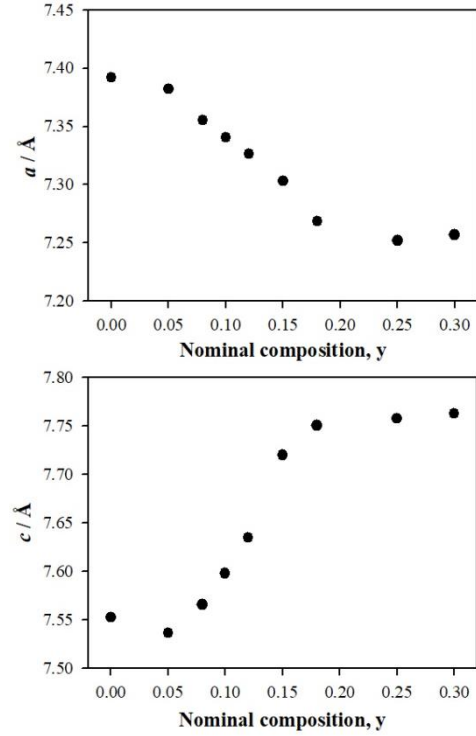


Fig.4a. Lattice parameters (a , c) of $\text{Rb}_{0.30}\text{V}_y\text{W}_{1-y}\text{O}_3$ ($0.0 \leq y \leq 0.30$) as a function of nominal composition, y .

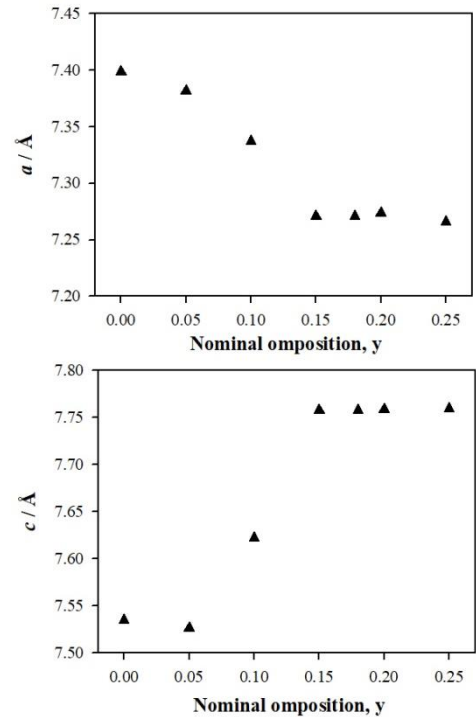


Fig.4b. Lattice parameters (a , c) of $\text{Rb}_{0.25}\text{V}_y\text{W}_{1-y}\text{O}_3$ ($0.0 \leq y \leq 0.25$) as a function of nominal composition, y .

The change in cell parameters of some pentavalent M^{5+} doped bronzes is compared in Table 2. This comparison shows that when 50% ($y = 0.15$) of W^{5+} are replaced the

cell parameters are noticeably changed for V compared to Ta substituted bronzes. This could be due to the difference of their ionic size. Since Ta^{5+} (0.73\AA) has larger size compared to V^{5+} (0.68\AA), the distortion (squeezing) of WO_6 octahedra is less prominent for tantalum when substituting larger W^{5+} (0.76\AA) ions.

Table 2. Comparison of cell parameter changes with a few structurally related systems.

HTB Phases	y	Decrease of cell Parameter, a (%)	Increase of cell Parameter, c (%)
$\text{K}_{0.30}\text{Ta}_y\text{W}_{1-y}\text{O}_3$ ²²		0.06	0.15
$\text{K}_{0.30}\text{V}_y\text{W}_{1-y}\text{O}_3$ ²¹	0.15	1.87	2.12
$\text{Rb}_{0.30}\text{V}_y\text{W}_{1-y}\text{O}_3$ (Present study)		1.69	2.45

It has been reported that for the system $\text{K}_x\text{Ta}_y\text{W}_{1-y}\text{O}_3$ cell parameters remains almost constant up to $y = 0.15$ and then a decreases and c increases as y increase further. Hussain et al.¹⁶, nevertheless, it was noted that in the Nb substituted HTB type $\text{K}_{0.30}\text{Nb}_y\text{W}_{1-y}\text{O}_3$ system cell parameters a and c both decreases with increasing nominal Nb content. It has been also reported that the lattice parameter a decreases and c increase up to $y = 0.15$ in the $\text{K}_x\text{V}_y\text{W}_{1-y}\text{O}_3$ system. With this information it could be concluded that there are some critical values for the substitution of pentavalent W by other pentavalent ions, which depends on the amount of W^{5+} ($= x$) in the initial composition. For example, in the case of $\text{Rb}_{0.30}\text{V}_y\text{W}_{1-y}\text{O}_3$ ($0 \leq y \leq 0.30$) and $\text{Rb}_{0.25}\text{V}_y\text{W}_{1-y}\text{O}_3$ ($0 \leq y \leq 0.25$) series, the limiting value of y are 0.18 and 0.15, respectively. Considering the ratio of $\text{V}^{5+}/\text{W}^{5+}$, it becomes $y/x = 0.18/0.30 = 0.60$ for the series $\text{Rb}_{0.30}\text{V}_{0.18}\text{W}_{0.82}\text{O}_3$ and also $y/x = 0.15/0.25 = 0.60$ for $\text{Rb}_{0.25}\text{V}_{0.15}\text{W}_{0.85}\text{O}_3$. This reveals that the vanadium doped hexagonal Rb_xWO_3 allow the contraction of the lattice when about 60% of the W^{5+} is replaced by V^{5+} and then with more incorporation of V^{5+} the structure remains rigid and shows other non bronze phases along with doped HTB phase. Previous Investigation^{16,22,23} reports on hexagonal $\text{K}_x\text{Nb}_y\text{W}_{1-y}\text{O}_3$, $\text{Rb}_x\text{Nb}_y\text{W}_{1-y}\text{O}_3$, $\text{K}_x\text{V}_y\text{W}_{1-y}\text{O}_3$ and $\text{K}_x\text{Ta}_y\text{W}_{1-y}\text{O}_3$ systems also show that about 50-60% W^{5+} could only be substituted by the respective pentavalent ions such as Nb^{5+} and Ta^{5+} , i.e., the limiting value is about 60%.

FTIR Spectroscopic Study

Infrared absorption spectra of polycrystalline samples of the series $\text{Rb}_{0.30}\text{V}_y\text{W}_{1-y}\text{O}_3$ and $\text{Rb}_{0.25}\text{V}_y\text{W}_{1-y}\text{O}_3$ measured at room temperature are depicted in Fig. 5. The spectra are measured in the 50 cm^{-1} to 4000 cm^{-1} range. Spectra above 1250 cm^{-1} are featureless (not shown in figures). For comparison, each figure includes the IR absorption spectra

of WO_3 (monoclinic, room temperature). The observer bands for WO_3 centered at 756 and 824 cm^{-1} are due to the symmetric and asymmetric stretching vibration of the W-O-W groups respectively in WO_6 octahedra.

The samples without vanadium, i.e., for nominal composition $y = 0.0$, exhibit no significant phonon absorption. The featureless rise in intensity with rising wavenumber due to metallic-like behavior of samples, which may be described as proportional to $(1-R)$, where R is the reflectivity. Similar results have been published for the Ta doped HTB system²². When W^{5+} ions are gradually replaced by V^{5+} , there is an absorption feature that develops as a function of y and exhibits a significant rise in intensity.

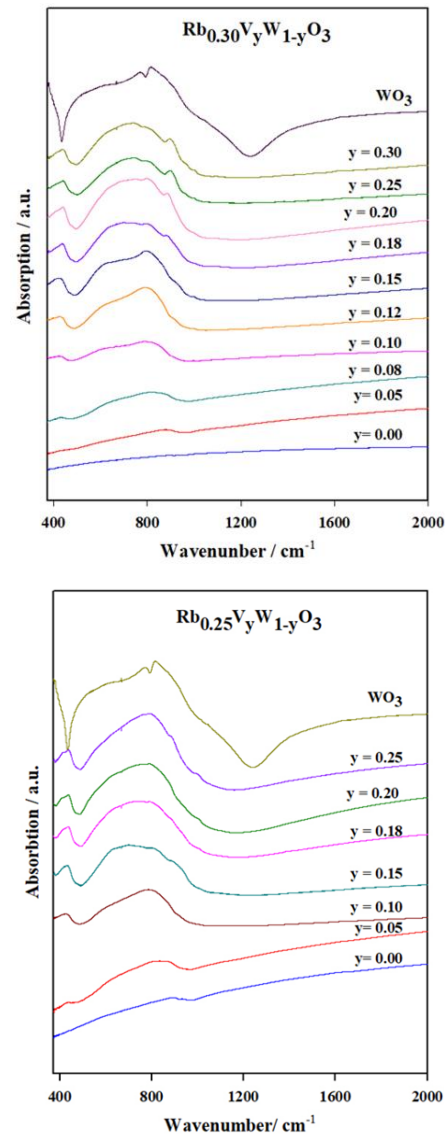


Fig. 5. FT-IR absorption spectra of the $\text{Rb}_{0.30}\text{V}_y\text{W}_{1-y}\text{O}_3$ and $\text{Rb}_{0.25}\text{V}_y\text{W}_{1-y}\text{O}_3$ series.

This increased phonon absorption intensity implies a significant decrease in the metallic like contribution and reveals nonmetallic nature of the compounds. The spectra obtained for the sample $\text{Rb}_x\text{V}_y\text{W}_{1-y}\text{O}_3$ correspond well with the powder-related spectra published by Dey *et al.*²¹. Additionally, some weaker bands are also observed in the same region. These weak bands may observe as a result of symmetry lowering of the distorted WO_6 octahedra in $\text{Rb}_x\text{V}_y\text{W}_{1-y}\text{O}_3$, which leads to lifting of degeneracy and relaxation of selection rules. This systematic distortion of WO_6 gives a clear indication to the vanadium doping to the investigated system.

Due to the large broadening of the bands of such reduced polycrystalline samples their actual assignment is very difficult. Maczka *et al.*³⁰ suggested that this problem can be avoided in the studies of their corresponding hexatungstates in which relatively sharp peaks are observed. Brusetti *et al.*²⁹ carried out a detail investigation of oxidation process of rubidium bronzes Rb_xWO_3 and found that at high rubidium content ($0.33 \leq x \leq 0.28$) hexatungstate is formed in equilibrium with impoverished HTB phase. Therefore, some of the selected samples of $\text{Rb}_{0.30}\text{V}_y\text{W}_{1-y}\text{O}_3$ were heated in air at 700°C to form corresponding hexatungstate. The oxidation of bronzes involves the conversion of all W^{5+} to W^{6+} . The structure of the samples was checked taking XRD and reveals the HTB type phase. The IR spectra of some these oxidized samples of the series $\text{Rb}_{0.30}\text{V}_y\text{W}_{1-y}\text{O}_3$ ($y = 0.10, 0.15, 0.20$ and 0.25) are compared with rubidium hexatungstate ($y = 0.0$) in Fig. 6. It can be seen the two most intense band at 813 cm^{-1} and 870 cm^{-1} are systematically shifted in low and high wave numbers respectively with increasing vanadium content.

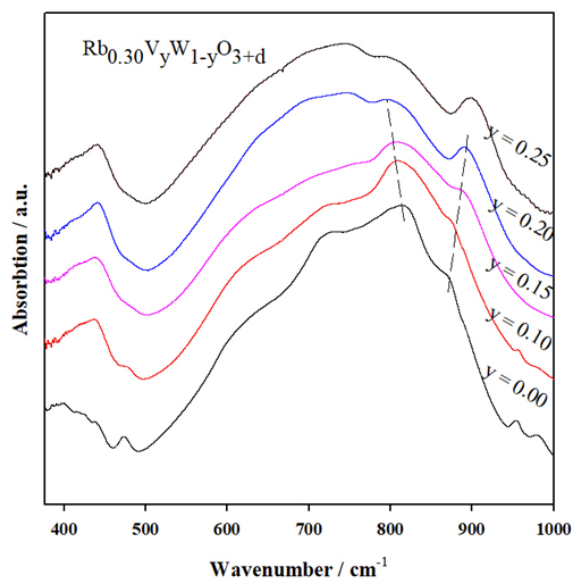


Fig. 6. FT-IR absorption spectra of some selected samples of the $\text{Rb}_{0.30}\text{V}_y\text{W}_{1-y}\text{O}_3$ series calcined 700°C in air. For clarity the spectra are plotted vertically.

According to Maczka *et al.*³⁹ the band at 870 cm^{-1} in polycrystalline Rb- hexatungstate is connected with vibrations of equatorial oxygen atoms, i.e. the atoms which form W-O bonds within the pseudo-hexagonal xy layers. The IR band at about 813 cm^{-1} is related with the vibrations of axial oxygen atoms forming W-O bonds, which are approximately perpendicular to the pseudo-hexagonal layers. Therefore, the shifting of these bands indicates that the V/W-O bond distances decreases in xy plane and increase in crystallographic c direction in their corresponding oxidized phase with increasing vanadium content. Since they are structurally related to their reduced phase, this result is consistent to our XRD results found for reduced $\text{Rb}_{0.30}\text{V}_y\text{W}_{1-y}\text{O}_3$ system. Rietveld refinement fit of the XRD data also reveals that average V/W-O distances within the xy plane decrease and the respective V/W-O distance along the crystallographic c direction increases as a result of substitution of W^{5+} by V^{5+} . Therefore, IR band shifting of the V/W-O stretching mode should be opposite in two directions, which is evident in Fig. 6.

SEM / EDX analysis

The morphology of the samples was examined using scanning electron microscopy, which shows the presence of hexagonal shaped crystals along with irregular shaped crystals.

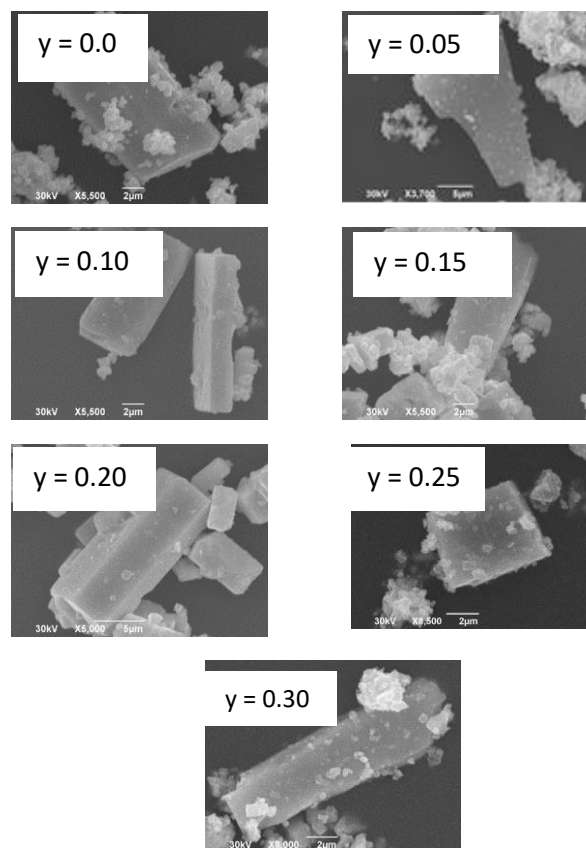


Fig. 7. SEM images of $\text{Rb}_{0.30}\text{V}_y\text{W}_{1-y}\text{O}_3$ series.

To evaluate the elemental composition, energy dispersive X-ray spectroscopy (EDX) was used. The spectra clearly reveal the presence of all experimental elements (O, Rb, W and V) in the samples, $\text{Rb}_{0.30}\text{W}_{1-y}\text{V}_y\text{O}_3$. The quantitative estimation was carried out counting the peak areas of the respective elements using JEOL software. Although the EDX study showed that the rubidium and vanadium content vary from crystal to crystal, their mean values are expected to be close to their nominal ones. Using 10 to 12 examined crystals from each sample, Table 2 provides the mean value of x and y . Table 3. shows that the composition of vanadium, y obtained from the EDX study reveals good agreement with their nominal values demonstrating systematic incorporation of vanadium in $\text{Rb}_x\text{V}_y\text{W}_{1-y}\text{O}_3$ system. To check the homogeneity of the elemental composition in crystals SEM/ EDX line scan were performed. As a typical example SEM/EDX line scan of a crystal with nominal composition $x = 0.30$, $y = 0.18$ is relative shown in Fig. 8. The intensities of each element remain constant throughout the length of the crystal indicating the compositional homogeneity.

Table 3. The mean values of x and y in the samples, $\text{Rb}_x\text{V}_y\text{W}_{1-y}\text{O}_3$ obtained from EDX analysis.

Nominal composition	Mean value of x	Mean value of y
$\text{Rb}_{0.30}\text{WO}_3$	0.33 (3)	-----
$\text{Rb}_{0.30}\text{V}_{0.05}\text{W}_{0.95}\text{O}_3$	0.31 (2)	0.049 (6)
$\text{Rb}_{0.30}\text{V}_{0.10}\text{W}_{0.90}\text{O}_3$	0.29 (3)	0.10 (2)
$\text{Rb}_{0.30}\text{V}_{0.15}\text{W}_{0.85}\text{O}_3$	0.30(2)	0.15 (2)
$\text{Rb}_{0.30}\text{V}_{0.20}\text{W}_{0.80}\text{O}_3$	0.29 (3)	0.19 (3)
$\text{Rb}_{0.30}\text{V}_{0.25}\text{W}_{0.75}\text{O}_3$	0.32 (2)	0.24 (3)
$\text{Rb}_{0.30}\text{V}_{0.30}\text{W}_{0.70}\text{O}_3$	0.29 (3)	0.28 (4)

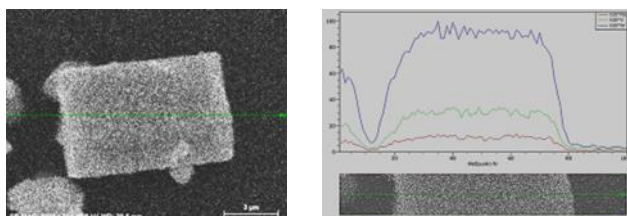


Fig. 8. Line scan of SEM / EDX to check the homogeneity of the elemental composition in a single crystal with $x = 0$, $y = 0.18$.

IV. Conclusion

Two series of polycrystalline samples were synthesized using the solid state synthesis method in an evacuated silica glass tube at 700°C , with nominal compositions of $\text{Rb}_{0.30}\text{V}_y\text{W}_{1-y}\text{O}_3$ ($y = 0.0 - 0.30$) and $\text{Rb}_{0.25}\text{V}_y\text{W}_{1-y}\text{O}_3$ ($y = 0.0 - 0.25$) respectively. X-ray powder diffraction, FTIR spectroscopy as well as Energy dispersive X-ray (EDX) and

Scanning Electron Microscopy (SEM) were used to characterize the products. XRD data in $\text{Rb}_{0.30}\text{V}_y\text{W}_{1-y}\text{O}_3$ series show that the pure hexagonal tungsten bronze (HTB) type phase can be prepared with compositions $y \leq 0.18$. The samples with $y \geq 0.20$, however, show the presence of small amount of other phases along with HTB. The cell parameters refined using space group P63/mcm show that a decreases up to $y = 0.18$, and then remains constant as y increase further. But c slightly decreases up to $y = 0.05$, then increases linearly as y increases from 0.05 to 0.18. For further increase in y , both cell parameters (a and c) remain nearly constant. This change in cell parameters indicates that the partial replacement of W atoms by V results in shortening of the W-W distances within the xy plane and elongation in the crystallographic c direction. SEM-EDX analysis also shows the systematic vanadium incorporation in the samples. Almost similar trend was obtained for $\text{Rb}_{0.25}\text{V}_y\text{W}_{1-y}\text{O}_3$ system. In this series, however, the pure HTB phase was obtained for $y \leq 0.15$. The spectroscopic data of the samples also support the successful incorporation of vanadium in the system.

Acknowledgements

Tapas Debnath thanks the “Deutscher Akademischer Austauschdienst (DAAD)” for providing the research fellowship, 2015 in the Institute of Mineralogy, Leibniz University of Hannover, Germany. The University Grand Commission, Bangladesh and Dhaka University are highly acknowledged for financial support in the project on Rb/Cs-HTB. Thanks to Higher Education Quality Enhancement Project (HEQEP) for the sub-project (CP-231).

References

1. Labbe, P. Tungsten Oxides, 1992. Tungsten Bronzes and Tungsten Bronze-Type Structures. *Key Eng. Mater.*, **68**, 293.
2. Raub, C. J., A. R. Sweedler, M. A. Jensen, S. Broadston and B. T. Matthias, 1964. Superconductivity of Sodium Tungsten Bronzes. *Phys. Rev. Lett.*, **13(25)**, 746.
3. Brigitte Krause, H., R. Vincent and J. W. Steeds, 1988. Microstructures in non-stoichiometric potassium tungsten bronzes K_xWO_3 . *Solid State Commun.*, **68(10)**, 937-942.
4. Liu, J. X., F. Shi, X. L. Dong, Q. Xu, S. Yin and T. Sato, 2013. Nanocrystalline Cs_xWO_3 particles: effects of N_2 annealing on microstructure and near-infrared shielding characteristics. *Materials characterization.*, **84**, 182-187.
5. Liu, G., S. Wang, Y. Nie, X. Sun, Y. Zhang, and Y. Tang, 2013. Electrostatic-induced synthesis of tungsten bronze nanostructures with excellent photo-to-thermal conversion behavior. *Journal of Materials Chemistry A.*, **1(35)**, 10120-10129.
6. Zhang, Y., Li, B., Y. Cao, J. Qin, Z. Peng, Z. Xiao, X. Huang, R. Zou and J. Hu, 2015. $\text{Na}_{0.3}\text{WO}_3$ nanorods: a multifunctional agent for in vivo dual-model imaging and photothermal therapy of cancer cells. *Dalton Transactions.*, **44(6)**, 2771-2779.
7. Tian, G., X. Zhang, X. Zheng, W. Yin, L. Ruan, X. Liu, L. Zhou, L. Yan, S. Li, Z. Gu and Y. Zhao, 2014. Multifunctional Rb_xWO_3 Nanorods for Simultaneous Combined Chemo-

- photothermal Therapy and Photoacoustic/CT Imaging. *Small.*, **10(20)**, 4160-4170.
8. Hägg, G., 1935. Zur Kenntnis der kubischen Natrium—Wolfram-Bronzen. *Zeitschrift für Physikalische Chemie.*, **29(1)**, 192-204.
 9. Magnéli, A., R. Mårin, C.M. Haug, J. Stene and N.A. Sörensen, 1951. Tetragonal tungsten bronzes of degenerated perovskite type. *Acta Chem. Scand.*, **5**, 670-672.
 10. Magnéli, A., 1949. The crystal structure of tetragonal potassium tungsten bronze. *Ark. Kemi.*, **1(24)**, 213-21.
 11. Magnéli, A., 1953. Studies on the hexagonal tungsten bronzes of potassium, rubidium and cesium. *Acta chem. scand.*, **7(2)**, 315-324.
 12. Hussain, A. and L. Kihlberg, 1976. Intergrowth tungsten bronzes. *Acta Crystallographica Section A: Crystal Physics, Diffraction, Theoretical and General Crystallography*, **32(4)**, 551-557.
 13. Hussain, A., 1978. Phase analysis of potassium, rubidium and cesium tungsten bronzes. *Acta Chem. Scand. A*, **32(6)**, 479.
 14. Cheng, K. H., A. J. Jacobson and M.S. Whittingham, 1981. Hexagonal tungsten trioxide and its intercalation chemistry. *Solid State Ionics.*, **5**, 355-358.
 15. Hussain, A., 1978. On the alkali metal tungsten bronzes, in particular those of potassium, rubidium and cesium (Doctoral dissertation, Stockholm University).
 16. Hussain, A., A. Ul-Monir, M. Murshed and C. H. Rüscher, 2002. Synthesis and characterization of niobium substituted hexagonal tungsten bronzes. *Zeitschrift für anorganische und allgemeine Chemie.*, **628(2)**, 416-420.
 17. Deschanvres, A., M. Frey, B. Raveau and JC THOMAZEA 1968. Substitution of tungsten by tantalum and niobium in potassium tungstates. Evidence for new phases $K_x(Nb_xW_{1-x})O_3$. $K_x(Ta_xW_{1-x})O_3$. *BULLETIN DE LA SOCIETE CHIMIQUE DE FRANCE.*, **(9)**, 3519.
 18. Galasso, F., L. Katz and R. Ward, 1959. Tantalum analogs of the tetragonal Tungsten bronzes. *Journal of the American Chemical Society.*, **81(22)**, 5898-5899.
 19. Debnath, T., C.H. Rüscher, T.M. Gesing, J. Koepke and A. Hussain, 2008. Solid-state synthesis in the system $Na_{0.8}Nb_yW_{1-y}O_3$ with $0 \leq y \leq 0.4$: A new phase, $Na_{0.5}NbO_{2.75}$, with perovskite-type structure. *Journal of Solid State Chemistry.*, **181(4)**, pp.783-788.
 20. Debnath, T., S.C. Roy, C.H. Rüscher, and A. Hussain, 2009. Synthesis and characterization of niobium-doped potassium tetragonal tungsten bronzes, $K_xNb_yW_{1-y}O_3$. *Journal of materials science.*, **44**, 179-185.
 21. Dey, K.R., T. Debnath, C.H. Rüscher, M. Sundberg, and A. Hussain, 2011. Synthesis and characterization of niobium doped hexagonal tungsten bronze in the systems, $Cs_xNb_yW_{1-y}O_3$. *Journal of materials science.*, **46**, 1388-1395.
 22. Shakil, M.M.R., T. Debnath, C.H. Ruscher and A. Hussain, 2012. Study of tantalum substituted potassium tungsten bronzes. *Journal of the Bangladesh Chemical Society.*, **25(1)**, 38-45.
 23. Abdullah, A.M., T. Debnath, C.H. Rüscher and A. Hussain, 2012. Synthesis and characterization of vanadium substituted potassium tungsten bronzes, $K_xV_yW_{1-y}O_3$. *Journal of Scientific Research 4 (2012), Nr. 2., 4(2)*, 507.
 24. Magnéli, A., 1989. 12th European Crystallographic Meeting.
 25. Skokan, M.R., W.G. Moulton, and R.C. Morris, 1979. Normal and superconducting properties of Cs_xWO_3 . *Physical Review B.*, **20(9)**, 3670.
 26. Stanley, R.K., R.C. Morris and W.G. Moulton, 1979. Conduction properties of the hexagonal tungsten bronze, Rb_xWO_3 . *Physical Review B.*, **20(5)**, 1903.
 27. Cadwell, L.H., R.C. Morris and W.G. Moulton, 1981. Normal and superconducting properties of K_xWO_3 . *Physical Review B.*, **23(5)**, 2219.
 28. Krause, H.B., W.G. Moulton and R.C. Morris, 1985. Investigation of superlattices in K_xWO_3 in relation to electric transport properties. *Acta Crystallographica Section B: Structural Science.*, **41(1)**, 11-21.
 29. Brusetti, R., P. Bordet and J. Marcus, 2003. Investigation of the Rb–W–O system in connexion with the superconducting properties of the hexagonal tungsten bronzes. *Journal of solid state chemistry.*, **172(1)**, 148-159.
 30. Mączka, M., J. Hanuza, and A. Waśkowska, 2003. Vibrational studies of alkali metal hexatungstates. *Journal of Raman Spectroscopy.*, **34(6)**, 432-437.
 31. STEFANOVICH, S., Z. Bazarova, I.S. Batueva and M.V. Mokhosoev, 1990. Polymorphism of oxides $Me_2MW_{15}O_{18}$ (Me= K, Rb, Cs, Tl; M= Ti, Zr, Hf) with the structure of hexagonal tungsten bronze. *Soviet physics. Crystallography*, **35(5)**, 692-694.
 32. King, C.N., J.A. Benda, R.L. Greene, and T. H. Geballe, 1972. Specific heat, optical, and transport properties of hexagonal tungsten bronzes. In *Low Temperature Physics-LT 13: Volume 3: Superconductivity* (pp. 411-415). Boston, MA: Springer US.
 33. Lynch, D.W., R. Rosei, J.H. Weaver and C.G. Olson, 1973. The optical properties of some alkali metal tungsten bronzes from 0.1 to 38 eV. *Journal of Solid State Chemistry.*, **8(3)**, 242-252.
 34. Rüscher, C.H., K.R. Dey, T. Debnath, I. Horn, R. Glaum, and A. Hussain, 2008. Perovskite tungsten bronze-type crystals of Li_xWO_3 grown by chemical vapour transport and their characterisation. *Journal of Solid State Chemistry*, **181(1)**, 90-100.
 35. Debnath, T., 2008. Structure, chemical composition and optical property relationship of alkali-metal tungsten oxides and niobium tungsten oxides. (Doctoral dissertation, Hannover: Gottfried Wilhelm Leibniz Universität).
 36. Paul, S., A. Ghosh, A. Chakraborty, L. Petaccia, D. Topwal, D. D. Sarma, S. Oishi and S. Raj, 2012. Temperature dependent photoemission spectroscopy on lightly-doped sodium tungsten bronze. *Solid state communications.*, **152(6)**, 493-496.
 37. Liu, S.J., H.W. Fang, Y.T. Su and J.H. Hsieh, 2014. Metal–insulator transition characteristics of Mo- and Mn-doped VO_2 films fabricated by magnetron cosputtering technique. *Japanese Journal of Applied Physics.*, **53(6)**, p.063201.
 38. Gesing, T.M., C.H. Rüscher and A. Hussain, 2001. Crystal structure of rubidium niobium tungsten bronzes, $Rb_xNb_yW_{1-y}O_3$ ($x \sim 0.3$; $y = 0.13, 0.19$). *Zeitschrift für Kristallographie-New Crystal Structures*, **216(1-4)**, 37-38.
 39. Maczka, M., J. Hanuza and A. Majchrowski, 2001. Vibrational properties of ferroelectric hexagonal tungsten bronzes $AB_xW_3-xO_9$, where A= K, Rb, Cs and B= Nb, Ta, Zr, Cr. *Journal of Raman Spectroscopy*, **32(11)**, 929-936.